Environmental Science and Pollution Research (2021) 28:36585–36597
https://doi.org/10.1007/s11356-021-13286-x

RESEARCH ARTICLE

Biochar derived from chicken manure as a green adsorbent for naphthalene removal

Chenchen Liu[1] · Zhihong Yin[1] · Dan Hu[1] · Fan Mo[1] · Ruoyu Chu[1] · Liandong Zhu[1,2] · Chaozhen Hu[1]

Received: 27 August 2020 / Accepted: 1 March 2021 / Published online: 11 March 2021

Abstract

In this study, biochar was generated from chicken manure by using a tube furnace under different temperatures (300, 500, and 700 °C), and the treatments were noted as J300, J500, and J700, respectively. In comparison, another type of biochar was prepared under 500 °C with a muffle furnace, and the treatment was noted as JM500. Biochar in treatment group J500 was subsequently modified with HNO_3 and NaOH, and the treatments were noted as J500-HNO_3 and J500-NaOH, respectively. The sorption efficiencies of naphthalene by the above six types of biochar were evaluated. Characteristic results showed that the surface pores of the biochar were improved with the increase of temperature, and biochar under the treatments J300, J500, J700, and JM500 experienced a high speed of adsorption within 1 h after the naphthalene adsorption started. The adsorption capacity of naphthalene increased with the increase of the initial concentration of naphthalene. Treatment J700 exhibited the largest adsorption capacity since its biochar surface pore structure was more fully developed with a crystal structure formed, and its specific surface area was increased by about 20 times compared to the original chicken manure. After biochar modification using HNO_3 and NaOH, the infrared spectrum changed, and the adsorption active sites were increased. The biochar modification by HNO_3 had a high naphthalene adsorption efficiency compared to NaOH. The order of adsorption capacity was as follows: J500 ≈ JM500 < J300 < J500-NaOH < J500-HNO_3 < J700.

Keywords Chicken manure · Biochar · Naphthalene · Removal · Adsorption

Introduction

The advance of industrialization increased the organic and inorganic pollution to the natural environment. Polycyclic aromatic hydrocarbons (PAHs) are volatile hydrocarbons, produced from coal, petroleum, wood, tobacco, organic polymer compounds, and other organic substances that are not completely burned. The generation of PAHs is one of the main contamination sources in the environment (Liu et al. 2014). PAHs are hydrocarbons containing more than two benzene rings in the molecule, including more than 150 compounds such as naphthalene, anthracene, phenanthrene, and fluorene (Zhang et al. 2004). Some PAHs also contain nitrogen, sulfur, and cyclopentane. Common PAHs with carcinogenic effects are mostly four to six ring-fused-ring compounds (Lamichhane et al. 2016). Naphthalene, as the most important fused aromatic hydrocarbon in industry, is produced in large quantities during coal tar coking and petroleum distillation (Fernandes et al. 2017). The physical and chemical properties of naphthalene are stable, non-degradable, and highly toxic, and they are considered as carcinogens, teratogens, and mutagens (Zhou et al. 2013). A secondary pollutant is generated after naphthalene releases into the surface water body through various reactions in environmental species (Dai et al. 2013), which seriously endangers human health and environmental safety (Zhu et al. 2019). It has been reported that naphthalene pollution increases the risk of human laryngeal cancer and colorectal cancer (Meng et al. 2019). Therefore, it is urgent

Responsible Editor: Zhihong Xu

✉ Liandong Zhu
ldzhu@whu.edu.cn

✉ Chaozhen Hu
chaozhenhu@126.com

[1] School of Resource and Environmental Sciences, Hubei Key Laboratory of Biomass-Resources Chemistry and Environmental Biotechnology, and Hubei International Scientific and Technological Cooperation Base of Sustainable Resource and Energy, Wuhan University, Wuhan 430079, P.R. China

[2] Faculty of Technology and Innovation, and Vaasa Energy Institute, University of Vaasa, P.O. Box 700, FI-65101 Vaasa, Finland

to use economical and effective means to control naphthalene pollution.

Naphthalene removal methods commonly used include oxidation (Peluffo et al. 2018), electrochemical treatment (Gómez et al. 2010), biodegradation (Shi et al. 2018), and adsorption (Zhou et al. 2013; Harmsen and Rietra 2018). The physical adsorption method is a green and economical method, which can adapt to changing water quality without secondary pollution, and the adsorbent can be recovered (Wu et al. 2013). The adsorption method refers to a process in which the adsorbate is adsorbed onto the surface of the adsorbent, thereby reducing the concentration of the adsorbate. The adsorption effect mainly depends on the nature of the adsorbent (Zheng et al. 2013a). Economical and efficient adsorbents include ion exchange resins, biomimetic adsorbents, and biochar (Ncube et al. 2018).

Biochar is a porous material formed by the pyrolysis of biomass under hypoxic or anaerobic conditions (Mohan et al. 2014). It has the characteristics of rich surface functional groups, high carbon contents, and multiple pore structures (Yin et al. 2018). It can be used as an alternative to activate carbon to adsorb organic or inorganic pollutants from aqueous solutions. As a new type of adsorbent, the properties of biochar are affected by the types of raw biomass materials, preparation processes, and technical parameters (Yao et al. 2012; Yin et al. 2018). The large specific surface area and porous structure of biochar facilitate the strong adsorption performance for the removal of pollutants. For example, biochar has been used to treat water soil pollutants as an effective sorbent, enhance fertility and food production as a soil amendment, and improve sewage sludge dewater ability as a skeleton structure. Therefore, the production of low-cost biochar adsorption materials for the treatment of environmental pollutants has become a hot topic (Zheng et al. 2013b). The pyrolysis temperature of biochar has a great influence on its properties and adsorption performances. Wei et al. (2019) revealed the molecular properties of biochar derived from Jerusalem artichoke stalks and found that its adsorption capacity to copper was closely related to the pyrolysis temperature. Xu et al. (2019) found an evident effect of pyrolysis temperature on the physicochemical properties of the biochar, including specific surface area, pH, and zeta potential. New biomass carbonization technology, which is involved with the production of biochar from wastes of agricultural products, has gradually attracted much attention.

With the social and economic development, the husbandry industry has developed tremendously, followed by the accumulation of fecal wastes. In China, about 250 million tons of feces are discharged every year (Mirheidari et al. 2019). Chicken manure is often added to agricultural soils as a soil fertilizer. It has been found that the combined effects of water conditions and the application of chicken manure might have a great potential capacity to reduce the simultaneous absorption of Cd and As by rice (Liu et al. 2019). Nowadays, in order to meet the demand for agricultural products, various additives such as hormones are added when feeding chickens (Patra and Saxena 2011). The antibiotics and excessive trace elements (heavy metals, especially Cu and Zn) are added into the feeds, but they cannot be completely metabolized by poultry, and thus most substances are excreted as feces. The release of feces will absolutely cause potential environmental problems. Both antibiotics and heavy metals threaten human health and environment (Li et al. 2019). If these feces are discharged directly without any treatment, they will cause serious pollution to aquatic environment and human beings. Currently, the generation of valuable products and the recycling and reusing of energy from livestock manure with simultaneously safe treatments are widely of concern. Among many methods for disposing livestock manure, pyrolysis for the generation of biochar presents obvious advantages, such as immobilization of heavy metals and nutrient recovery (Tian et al. 2019; Patra and Saxena 2011; Yargicoglu et al. 2014). Previous studies showed that heavy metals were successfully fixed onto the pyrolytic pig and sheep manure, and the higher the temperature, the better the performance (Zeng et al. 2018). Lin et al. (2017) studied the effects of various pyrolysis temperatures on the morphology, leaching rate, and bioavailability of copper and zinc in animal manure–derived biochar. As for chicken manure treatment, most previous studies have been done to produce biodiesel from chicken manure or generate methane by composing. The annual yield of chicken manure is so high that handling it is a problem, including heavy metals and organic contamination, which may produce secondary pollution. Therefore, biochar prepared by pyrolysis at high temperature can be used as an environmental adsorbent to remove pollutants. From the perspective of economy, the recycling of wastes also brings economic benefits. Thang et al. (2019) studied the adsorption application of chicken manure biochar toward 2,4-dinitrophenol and phenol, which showed excellent removal efficiencies. In addition to this, there is scarce research on developing the potential of chicken manure–derived biochar as adsorbent.

Owing to the lack of theoretical and experimental research on transforming chicken manure into biochar and use as low-cost adsorbent for water treatment, it is therefore a challenging task to develop a highly effective adsorbent with low secondary pollution and non-release of by-products, especially non-toxic to the environment, to remove organic pollutants such as naphthalene. However, as far as we know, there has been no research on the adsorption of naphthalene from wastewater using chicken manure biochar. The innovation of this study is to identify a new application of chicken manure biochar as adsorbent to remove toxic naphthalene from wastewater. This study also included concrete operation of the preparation of adsorbent, adsorption kinetics, and adsorption isotherm,

providing a basis for further large-scale practical application. The consequence of this study may be putting forward ideas for waste management to reduce environmental pollution in China.

In this study, chicken manure was selected as the raw material to produce biochar under various pyrolysis temperatures, and biochar produced was then utilized as the adsorbent of naphthalene. The present study was carried out with the following specific objectives: (1) to investigate the characteristics of biochar prepared from chicken manure under different temperatures by using SEM, BET, XRD, and FTIR; (2) to explore the kinetics and isotherm of naphthalene onto biochar; (3) to evaluate the characteristics and absorption mechanisms of modified biochars for naphthalene removal.

Materials and methods

Reagents and chemicals

Naphthalene was obtained from Sigma-Aldrich (Steinheim, Germany). Sodium azide (NaN_3) was purchased from Tianjin Baishi Chemical Industry Co., Ltd (China). Analytical-grade calcium chloride ($CaCl_2$), sodium hydroxide (NaOH), and nitric acid were purchased from Sinopharm Chemical Reagent Co., Ltd (China). HPLC-grade methyl alcohol was purchased from Anhui Tedia High Purity Solvents Co., Ltd (Anhui, China).

Chicken manure for the preparation of biochar

To produce biochar, chicken manure, which was viewed as breeding industry wastes, was selected as a biomass feedstock. The chicken manure was collected from Hubei Province (China), milled by using a pestle and mortar. The treated biomass material was pyrolyzed using a tubular furnace with a quartz boat in the presence of N_2. The material was pyrolyzed at a rate of 5 °C/min and then held for 2 h when the temperatures reached 300, 500, and 700 °C, respectively. The material was then cooled to room temperature and ground, passed through a 60-mesh sieve, and stored with plastic seal bags in a dry container. Based on the temperature applied, the biochar for the adsorption was designated as J300, J500, and J700.

The chicken manure was placed in a N_2-filled muffle oven at 500 °C for 2 h to produce biochar, cooled to room temperature and ground, and then passed through an 80-mesh sieve. The resulting biochar for the adsorption was designated as JM500.

Modification of biochar derived from chicken manure

Three grams of the chicken manure biochar which was prepared in a tube furnace under 500 °C was accordingly added into 30 mL of 8×10^4 mg/L NaOH solution and 65% HNO_3, respectively (Jin et al. 2018; Luo et al. 2018), in order to achieve the volume ratio of biochar mass to modified solution at 1:10. After the reaction in water bath under 60 °C for 2 h, the resulting biochar was stirred, filtered, and then rinsed with plenty of deionized water until the filtrate was neutral. The biochar was placed in the electric blast drying oven under 80 °C for 4 h, and then cooled to room temperature. Based on the modified method, the biochar for the adsorption was accordingly named as J500-NaOH and J500-HNO_3.

Characteristics determination

Scanning electron microscopy (SEM) (S4800; Hitachi, Japan) was used to identify the structural morphology of biochar samples. The structure and crystallinity of the sorbent was characterized by an X-ray diffractometer (XRD) (MiniFlex 600; Rigaku, Japan) with Cu Kα radiation at 40 kV and 30 mA in a 2θ range of 10–80°. Fourier transform infrared spectroscopy (FTIR) (Vertex70; Bruker, Germany) was undertaken using KBr in the range 400–4000 cm^{-1}. The specific surface area (SSA), pore size, and pore volume of each biochar sample were determined using the Brunauer–Emmett–Teller (BET) adsorption method by N_2 adsorption–desorption isotherm at 77.0 k (Belsorp-miniII; MicrotracBEL Corp, Japan).

Sorption experiments

Sorption kinetic experiments

The adsorption kinetics analysis was carried out by batch adsorption experiment. Then 0.05 g of each sample including J300, J500, J700, and JM500 was mixed with 25 mL of 10 mg/L naphthalene in a triangular flask. Each mixture contained $CaCl_2$ (1.11×10^3 mg/L) to hold constant ionic strength and NaN_3 (200 mg/L) to reduce microbial activity. The flasks were sealed and shaken at 150 rpm at a constant temperature shaker under 25 °C with the predetermined hours (0.5, 1, 2, 4, 8, 12, 18, 24, and 36 h). When shaking was completed, each triangular flask was taken out, and about 10 mL mixture was centrifuged at a rotation speed of 2000 rpm for 20 min. After the end of the centrifugation, the supernatant was filtered through a 0.45-μm filter, and 1.8 mL of the filtrate was injected into a 2-mL liquid phase sample bottle. In order to minimize the volatilization of naphthalene, the sample bottle was covered with tin foil and sealed. For the concentration analysis, the blank control sample was not filtered, and 1.8 mL was directly injected into the liquid phase sample bottle, and finally the mass concentration of naphthalene was measured by high-performance liquid chromatography (HPLC). Control tests were conducted without biochar addition under the same conditions. All experiments were conducted in triplicates, and

the mean value of the parallel experiment was taken for analysis.

Sorption isotherm experiments

Sorption isotherm experiments were conducted with the same procedures which were used for the sorption kinetics experiments. A series of naphthalene solutions with the initial concentrations of 2, 5, 10, 15, 20, 25, 30, 35, and 40 mg/L were prepared to perform the experiments. Then, parallel samples and blank control samples were set up, and the parallel experimental data were averaged for analysis. The different values of naphthalene content in the blank control samples and the experimental samples were used to accurately quantify the adsorption amount of naphthalene by biochar. All samples were shaken under 25 °C for 22 h at a speed of 150 rpm, in order to reach the sorption equilibration.

Data analysis

Adsorption kinetic model

Adsorption kinetic models were used to fit the adsorption process of chicken manure biochar for removing naphthalene, and the following three models were used to fit the adsorption kinetics process: pseudo-second-order kinetic model (2.1), Elovich model (2.2), and intra-particle diffusion model (2.3) (Wang et al. 2014).

$$t/q_t = 1/k_2 q_e^{\ 2} + t/q_e \tag{2.1}$$

$$q_t = a + bt \tag{2.2}$$

$$q_t = k_p t^{1/2} + c \tag{2.3}$$

where q_e and q_t are the adsorption amount of the adsorbent at equilibrium and at time t (mg/g), respectively; k_2 represents the standard second-order adsorption rate constant ($g \cdot mg^{-1} \cdot min^{-1}$), while k_p represents the internal diffusion rate constant ($g\ mg^{-1}\ min^{-1/2}$).

Adsorption isotherm model

The peak area of the sample was measured by HPLC and converted to the mass concentration of naphthalene, according to the standard curve.

The naphthalene adsorption capacity by biochar was calculated by mass balance equation as follows:

$$q_e = V \times (C_0 - C_e)/m \tag{2.4}$$

where q_e represents the equilibrium adsorption amount of naphthalene (mg/g); C_0 and C_e represent the initial and the equilibrium concentration in the solution (mg/L), respectively.

In the experiment, isothermal adsorption line model was adopted to analyze the adsorption mechanism of biochar, and the following three models were used to fit the isothermal adsorption line: linear model (2.5), Langmuir model (2.6), and Freundlich model (2.7) (Chen and Chen 2009).

$$q_e = K_d C_e + b \tag{2.5}$$

$$q_e = b q_m C_e/(1 + bC_e) \tag{2.6}$$

$$q_e = K_F C_e^{\ 1/n} \tag{2.7}$$

where q_e and q_m represent the equilibrium and maximum adsorption amount of the adsorbent (mg/g), respectively. C_e represents the equilibrium concentration in the solution (mg/L). K_d represents the linear distribution coefficient; K_F represents the capacity factor, indicating the adsorption capacity of solid adsorbent in a solution with a certain amount of adsorbent. $1/n$ represents an exponential factor, which can reflect the bending degree of adsorption isotherm. b is a constant.

Results and discussion

Biochar characteristics

Morphologies and BET surface area analysis

The surface morphology of biochar had transmuted obviously with the increase of pyrolysis temperature (Fig. 1). The surface of J300 was relatively smooth, and the pore structure was not yet developed. In contrast, micropores had begun to be developed on the surface of J500, and its pore structure was more obviously developed than J300 since more volatile components in chicken manure overflowed and formed small pores as the increase of temperature. When the temperature reached 700 °C, the micropores on the surface of J700 were well developed and a large diameter pore structure was also produced.

The SSA measurement was used for the characterization of different biochar types, and the results are exhibited in Table 1. The BET surface area of the chicken manure after pyrolysis treatment enlarged evidently, and the BET surface area gradually increased as the increase of pyrolysis temperature. The mean pore value of J700 was 6.25 nm, illustrating that the surface pores of J700 were mainly mesoporous.

The FTIR and XRD analysis

Fourier infrared spectra of the four biochar types before and after the adsorption of naphthalene are shown in Fig. 2a. J300-mix, J500-mix, JM500-mix, and J700-mix represent the mixed substances after the adsorption of naphthalene by J300, J500, JM500, and J700, respectively.

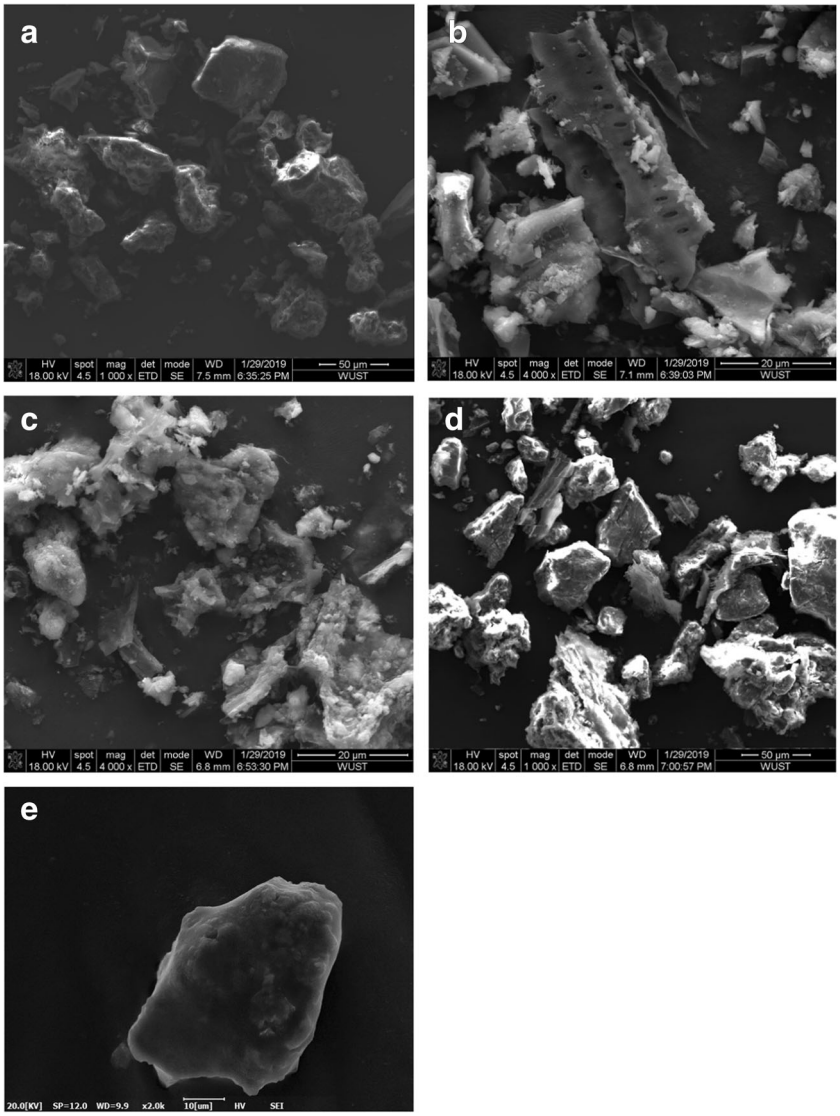

Fig. 1 The SEM images of **a** J300, **b** J500, **c** J700, **d** JM500, and **e** chicken manure

Analysis of the spectrum demonstrated that the four types of biochar kept similar groups of absorption peaks, and the specific ranges were: 690–880 cm^{-1}, 914–1220 cm^{-1}, 1342–1800 cm^{-1}, 2271–2400 cm^{-1}, and 2271–2400 cm^{-1}. The absorption peaks appeared around 1620 cm^{-1}, indicating the presence of C=C double bonds. The peak strength gradually decreased with the increase of pyrolysis temperature, and there was no such absorption peak in treatment J700. The aldehyde-based absorption peak was around 1430 cm^{-1}, and the peak strength also decreased as the increase of preparation temperature. The absorption peaks appearing between 1000 and 1100 cm^{-1} were related to the deformed C–H ring

Table 1 Basic physical properties of chicken manure, J300, J500, J700, and JM500

Adsorbent	Basic feature		
	BET surface area (m^2/g)	Pore volume (cm^2/g)	Pore size (nm)
Chicken manure	0.75	0.01	40.55
J300	1.51	0.02	38.81
J500	4.20	0.02	19.22
J700	15.48	0.02	6.25
JM500	2.97	0.02	37.87

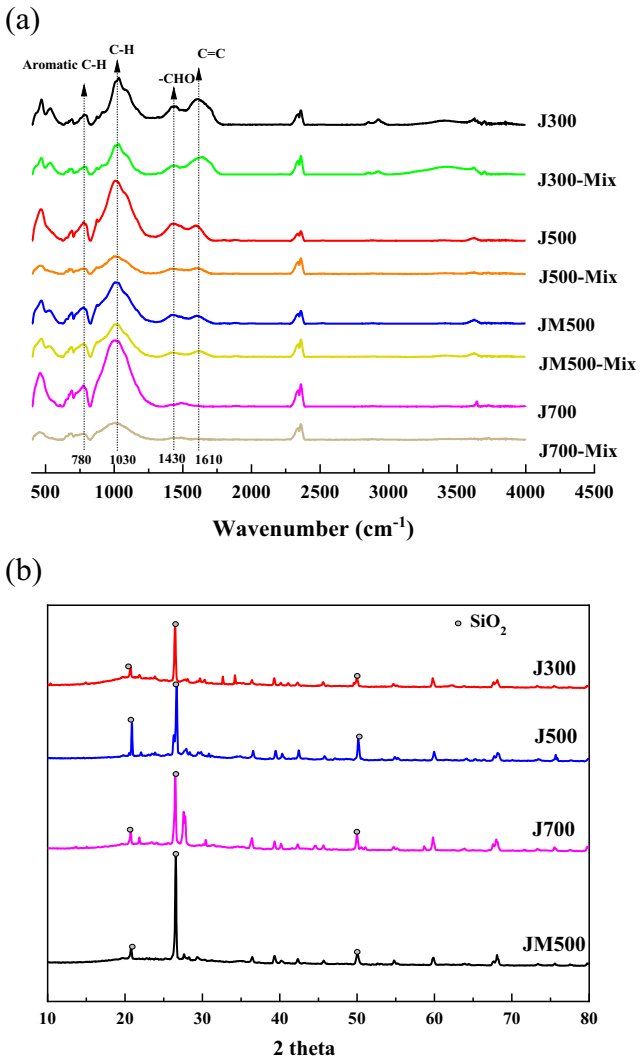

Fig. 2 **a** FTIR spectra of J300, J500, J700, and JM500 before and after absorption of naphthalene and **b** the XRD patterns of J300, J500, J700, and JM500

vibration peaks, and the order of the peak strength was J700 > J500 > J300 > JM500. The absorption peaks appearing at 690–880 cm^{-1} represented the vibration peaks of aromatic hydrocarbon compounds. In general, the frequency of peaks in the infrared spectra of the four types of biochar was not obviously different.

As shown in Fig. 3a, comparing the infrared spectra of the four types of biochar before and after the adsorption of naphthalene, the peak intensities at 690–880 cm^{-1} of J700-Mix and J500-Mix were evidently lower than J700 and J500, which means the adsorption of naphthalene affected their functional groups, and the aromatic C–H bond might be reduced. The peak strength of the J700-Mix at 1000–1100 cm^{-1} was obviously weakened than J700, while the peak wavenumber was increased, indicating that adsorption might occur on the C–H bond. The peak strength of J300, J500, and JM500 at 1620 cm^{-1} was decreased, and the wavenumber enlarged after adsorption, suggesting that the adsorption might occur on the C=C bond. The waveforms of the infrared spectra of biochar before and after the adsorption of naphthalene did not change, and none of the new peaks was generated. Meanwhile, several peaks shifted and the intensity changed, indicating that the intensity of the chemical bond might have been changed during the adsorption process (Keiluweit et al. 2010).

The crystal structure and contents of materials can be obtained by X-ray diffraction. As shown in Fig. 2b, the biochar of chicken manure created an obvious crystal structure, and the main phase was SiO_2. With the increase of pyrolysis temperature, the crystal structure of biochar derived from chicken manure did not experience an obvious change.

Sorption kinetics of naphthalene

As shown in Fig. 3, biochar J300 and J700 ended the fast adsorption process at about 4 h and reached the adsorption equilibrium within about 8 h during the absorption. In contrast, biochar J500 and JM500 basically completed the fast adsorption process at about 4 h, and basically reached an adsorption balance within 24 h. Therefore, the adsorption of naphthalene by chicken manure–based biochar preserved a fast and subsequently slow process. In the early stage of adsorption, the solution maintained high concentrations of naphthalene, and there were sufficient adsorption sites on the surface of the biochar (Hale et al. 2012). The biochar was in direct contact with the naphthalene molecules, which were adsorbed onto the surface of chicken manure–based biochar. It took a long time to diffuse into the internal space of biochar, so the adsorption rate became slower and finally reached the adsorption equilibrium (Kaur and Sharma 2019).

As shown in Table 2, as for the simulation of the Elovich model, because the correlation coefficients (R^2) fitted to the four biochar adsorption kinetic curves of this experiment were relatively small, the adsorption of naphthalene by chicken manure–based biochar was not suitable for this model. For the particle diffusion model simulation, the fit of the other types of biochar was poor except JM500, indicating that the adsorption of naphthalene by chicken manure–based biochars not only existed during particle diffusion but also were affected by other factors of adsorption mechanism (Freddo et al. 2012). For the fitting of the pseudo-second-order kinetic model, the value of R^2 was between 0.915 and 0.975, which indicated that the pseudo-second-order kinetic model was more suitable for the data fitting of the four types of biochar in this adsorption experiment, and the value of q_e was in line with the experimentally measured value. The actual values were relatively similar, and the order of their sizes was J500 ≈ JM500 < J300 < J700. This fitting result was consistent with the order of the adsorption capacity obtained in the isothermal adsorption experiment. The parameter k_2 represented the adsorption rate

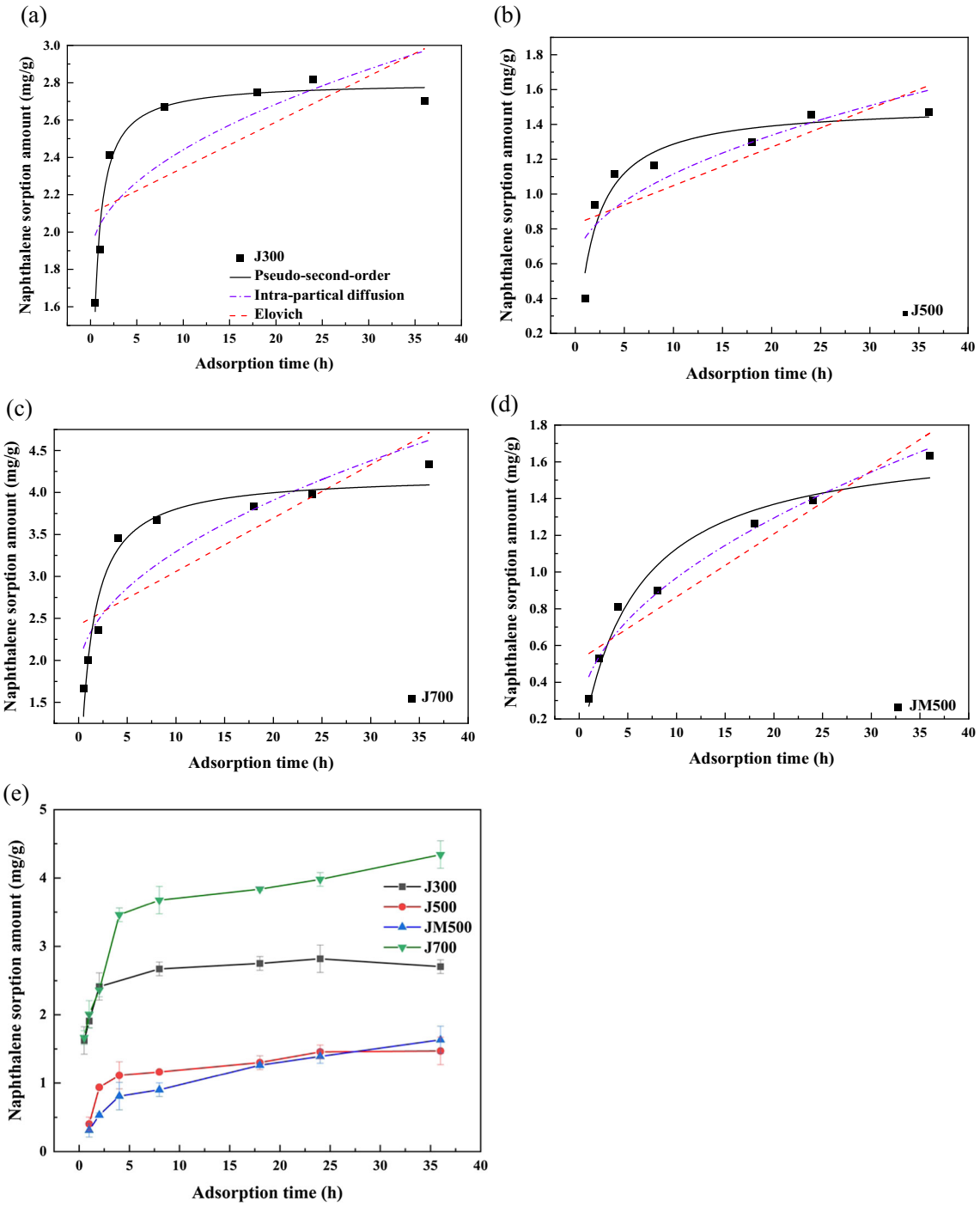

Fig. 3 Pseudo-second-order, intra-particle diffusion, and Elovich kinetics of naphthalene onto J300 (**a**), J500 (**b**), J700 (**c**), and JM500 (**d**). **e** Adsorption kinetic curves of naphthalene onto J300, J500, J700, and JM500

constant, and with the increase of the preparation temperature, k_2 was transformed obviously, which reflected that the fast adsorption was dominant in the adsorption process (Mukherjee et al. 2011). The results of the kinetic models were in great agreement with the study reported on the adsorption of naphthalene on activated carbon from sawdust (Kumar and Gupta 2020). The same results were found in another study, which shows that the Freundlich adsorption model was also suitable for kaolin/Fe_3O_4 composite to adsorb naphthalene (Mirbagheri and Chen 2019). This indicated that the adsorption process was related to the way the molecule contacted with adsorbed surface, the accessibility of the adsorbent surface, and the properties of the interactions between naphthalene and the adsorbent.

Table 2 Kinetic parameters obtained from three different models of naphthalene absorption

Absorbent	Pseudo-second-order kinetics			Elovich			Intra-particle diffusion		
	q_e	k_2	R^2	a	b	R^2	k_p	c	R^2
J300	2.804	0.912	0.975	2.099	0.025	0.418	0.186	1.851	0.628
J500	1.513	0.375	0.915	0.827	0.022	0.549	0.170	0.579	0.705
J700	4.213	0.220	0.941	2.422	0.064	0.626	0.468	1.815	0.801
JM500	1.742	0.105	0.956	0.522	0.034	0.885	0.249	0.182	0.970

The removal efficiency of the four types of biochar was calculated, and treatment J700 could adsorb 84.3% naphthalene from the solution which was the highest among the four types of biochar, followed by treatment J300 (56.1%), J500 (34.8%), and JM500 (30.3%). In a previous study, the naphthalene removal efficiency of activated carbon produced from flamboyant pod and milk bush kernel shell by different pyrolysis temperatures generally ranked around 40% (Abass Olanrewaju Alade 2012).

Sorption isotherms of naphthalene

The results of isothermal adsorption of naphthalene on four types of chicken manure–based biochar (J300, J500, J700, and JM500) are shown in Fig. 4. In this experiment, the relative parameters from the linear model, Langmuir model, and Freundlich model are listed in Table 3.

The parameter R^2 of the isothermal adsorption curve in Table 3 suggested that the linear models of the four types of biochar fitted J300 and J500, and the fitting of J700 and JM500 showed a poor correlation, testifying that it was not suitable for linear fitting. The R^2 values fitted by the four types of biochar to the Langmuir model ranged from 0.885 to 0.984. Except for J700, the R^2 values of the other three types of biochar reached above 0.95. The correlation coefficient of the four types of biochar to the Freundlich model was very high. Considering the comprehensive experimental data, the Freundlich model was the most suitable for fitting the four types of biochar for naphthalene adsorption. As shown in Fig. 4b, with the increase of the concentration of the adsorbate solution, the equilibrium concentration of adsorption increased, and the adsorption capacity of naphthalene also increased. The isothermal adsorption curves of the four types of biochar were all "L"-shaped curves (Mirheidari et al. 2019). Since the adsorption sites on biochar were completely occupied, it became increasingly difficult for the adsorbate to reach the surface adsorption sites of biochar (Prak and Pritchard 2002).

From the linear regression, it is known that the linear distribution coefficient value of J300 was 0.500, larger than that of J500 (0.137), proving that the adsorption of naphthalene by J300 was likely to maintain a distribution effect (Leng 2014). In the Langmuir model, the q_m value denotes the maximum adsorption capacity, and b represents the stability of the binding as well as the strength of the adsorption effect between the adsorbent and the adsorbate. The order of the two parameters was J700 > J300 > J500 > JM500. In the Freundlich model, K_F represented the capacity factor, and its order of magnitude was J700 > J300 > JM500 > J500. The valve of $1/n$ reflected the degree of curve bending, in other words, the degree of non-linearity, and its order of magnitude was J300 > J500 > JM500 > J700. As the decrease of the $1/n$ value, the stronger the binding stability between the adsorbate and the adsorbent, the more non-linearity might be caused by the combination of surface adsorption and distribution (Yin et al. 2019).

The Langmuir model was suitable for monomolecular layer adsorption fitted to a uniform surface, which belonged to a physical adsorption, while the Freundlich model was suitable for multimolecular layer adsorption fitted to an uneven surface, which belonged to a chemical adsorption. The adsorption mechanisms of J300, J500, and JM500 belonged to the single-molecule layer adsorption (Chen and Zhou 2008). All four types of biochar conserved the chemical adsorption. Comparing the chicken manure-based biochar prepared at 500 °C between the tube furnace and the muffle furnace, the adsorption performance kept a slight difference. Muffle furnace is not as air-tight as tube furnace, which might be the reason for the difference. The porosity of the biochar was changed by the existence of air in the pyrolysis environment, influencing its adsorption properties (Li et al. 2019).

Sorption mechanisms

In summary, chicken manure–based biochar prepared under different temperatures performed the various adsorption capacities of naphthalene, and J700 experienced the maximum adsorption capacity, followed by J300, and the worst effect was under 500 °C. According to the scanning electron microscope results, with the increase of the pyrolysis temperature, the microspores on the surface of biochar were improved. Thus, the distribution effect during the adsorption process was gradually weakened, while the pore filling effect was gradually increased. Under 300 and 500 °C, chicken manure was partially carbonized, and the partial

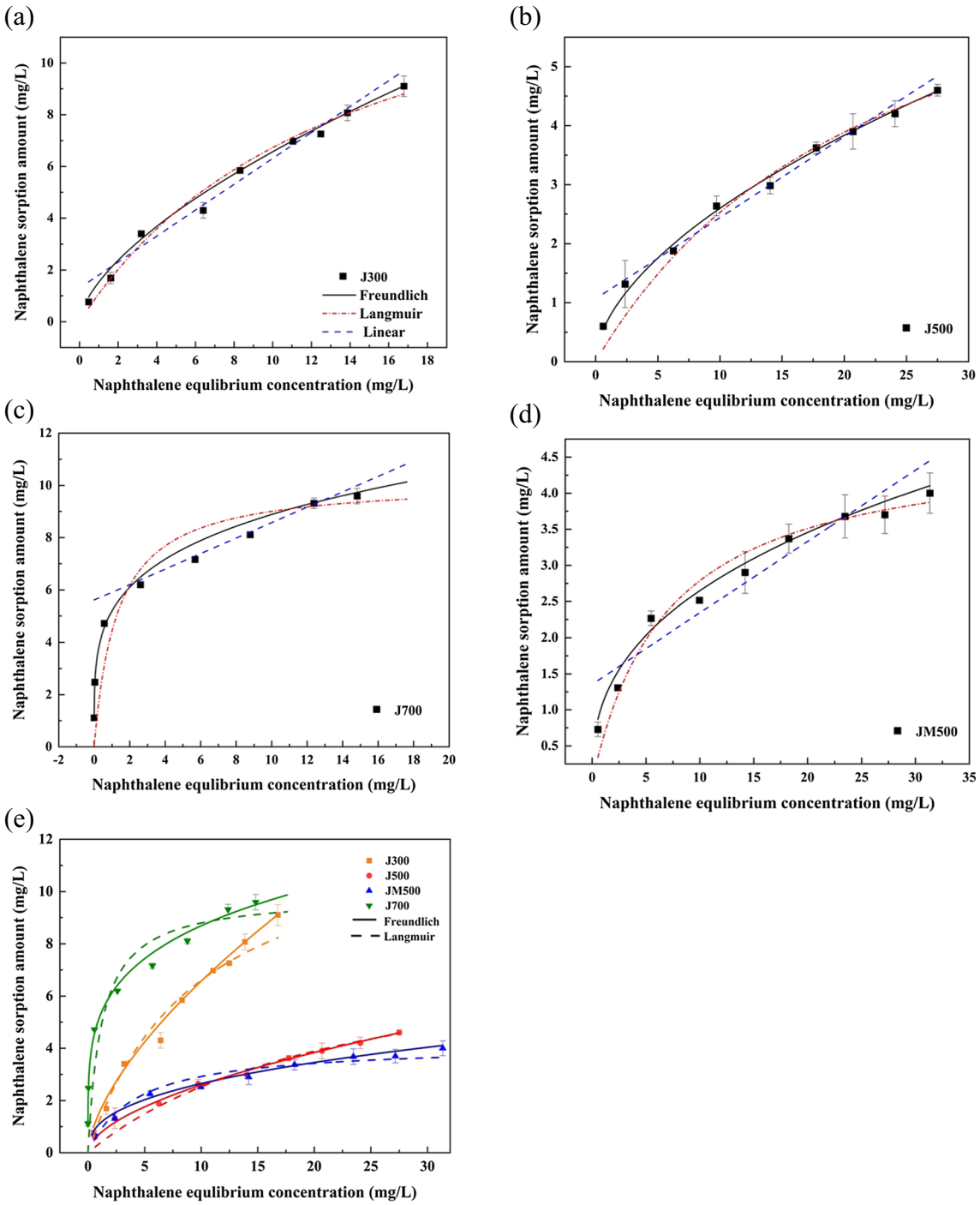

Fig. 4 Linear, Langmuir, and Freundlich isotherm models of naphthalene onto J300 (**a**), J500 (**b**), J700 (**c**), and JM500 (**d**). **e** Langmuir and Freundlich isotherm model of naphthalene onto J300, J500, J700, and JM500

carbonization mainly played a role of distribution absorption, while the surface adsorption was mainly attributed to the carbonized part. The carbonization was relatively completed under 700 °C. The adsorption was mainly micropore filling and surface adsorption. Studies had manifested that the mesoporous structure was suitable for adsorption, and the most suitable mesoporous structure was generated under a pyrolysis temperature of 700 °C (Li et al. 2019). It was speculated that the strongest adsorption capacity of J700 in this experiment might be due to the inclusion of both microporous and mesoporous structures. The pore development of J300 was incompletely carbonized, and the distribution was primarily adsorption mechanism. In contrast, the distribution of J500 was not as strong as J300, and the pore development was not as complete as J700, which caused the worst adsorption capacity.

Table 3 Linear, Langmuir, and Freundilich isotherm parameters for the adsorption of naphthalene onto J300, J500, J700, and JM500

Absorbent	Linear		Langmuir			Freundlich		
	K_d	R^2	q_m	b	R^2	K_F	$1/n$	R^2
J300	0.500	0.964	7.317	0.257	0.984	1.535	0.631	0.991
J500	0.137	0.977	6.919	0.206	0.968	0.711	0.562	0.994
J700	0.296	0.878	10.167	0.772	0.885	5.192	0.233	0.994
JM500	0.096	0.900	4.738	0.143	0.958	1.097	0.383	0.981

Adsorption of naphthalene by modified chicken manure biochar

Infrared spectrum characteristics of modified chicken manure–based biochar

Combining the adsorption isotherm with adsorption kinetics for the line fit analysis of the four types of biochar in previous sections, J500 with poor adsorption performances was selected as the modified material to improve its adsorption performance. The Fourier infrared spectra of the two types of modified biochar obtained by accordingly modifying J500 with acid (HNO_3) and alkali (NaOH) before and after naphthalene adsorption are shown in Fig. 5. As shown in Fig. 5, the intensity of the aldehyde group absorption peak at 1610 cm^{-1} of the biochar obtained by modification with NaOH increased and the wave enhanced, indicating that the modification increased the number of C=O groups of biochar and affected structural transformation. The intensity of the O–H absorption peak at 3430 cm^{-1} enlarged evidently, suggesting that the modification of NaOH might amplify the O–H functional group of biochar. The intensity of the C–OH peak at 1080 cm^{-1} was enhanced after HNO_3 modification. A new absorption peak, –COO–, was generated at around 1385 cm^{-1}, which might be generated by the strong oxidation of concentrated nitric acid. The strong oxidizing properties might also cause the appearance of a strong saturated C=O peak at 1710 cm^{-1}. Using NaOH to modify biochar, the intensity of the O–H absorption peak at 3430 cm^{-1} was obviously magnified.

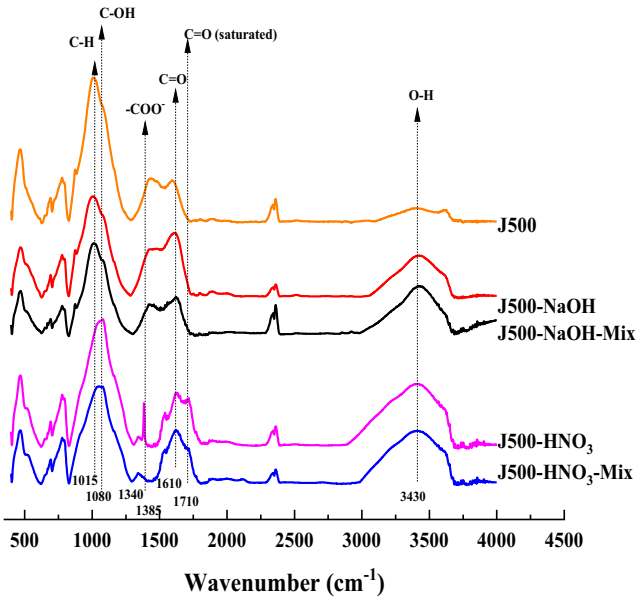

Fig. 5 FTIR spectra of J300, J500, J700, and JM500 before and after absorption of naphthalene

In addition, after the adsorption of naphthalene, there was no obvious change in the vibrational absorption peaks of the C–H bonds of aromatic hydrocarbons at 690–880 cm^{-1}, testifying that the adsorption of naphthalene by both types of modified biochar did not affect the aromatic hydrocarbon groups. However, the deformed C–H appeared at around 1015 cm^{-1}. The bond ring vibration peak was slightly shifted and the peak intensity was slightly reduced. Some naphthalene might be adsorbed onto biochar to convert its structure. The –COO– based absorption peak of J500-HNO_3 at 1385 cm^{-1} disappeared after the adsorption of naphthalene, which demonstrated that the –COO– group showed a great effect on the adsorption process of naphthalene (a chemical reaction might have occurred). The saturated C=O peak of J500-HNO_3 at a frequency of about 1710 cm^{-1} was significantly weakened, suggesting that a chemical reaction possibly occurred during the adsorption process. The intensity of the O–H absorption peak at 3430 cm^{-1} was expanded, which happened in both types of modified biochar, suggesting that naphthalene might be adsorbed onto the surface. In summary, the infrared spectrum of the biochar modified by HNO_3 experienced greater change, which particularly generated new functional group, –COOH–. Although J500-NaOH did not have new adsorption peaks, the functional groups on its surface were accumulated.

Isothermal adsorption of naphthalene by modified chicken manure-based biochar

Three isotherm models (linear, Langmuir, and Freundlich model) were used to fit the isotherm adsorption lines of naphthalene on two types of modified biochar, compared with the J500 biochar before modification. The parameters calculated from these isotherm models are exhibited in Table 4. The isothermal adsorption curves of the two types of modified biochar for naphthalene removal are shown in Fig. 6. According to the R^2 of the models, these three models could well fit the isotherm adsorption lines.

Comparing the adsorption performance of biochar before and after modification, it was found that the partition coefficients K_d of J500-HNO_3 and J500-NaOH were higher than that of J500, indicating that after modification the distribution and adsorption during the process became stronger. The q_m of the two types of modified biochar was higher than that before

Table 4 Linear, Langmuir, and Freundlich isotherm parameters for the adsorption of naphthalene onto J500-HNO_3, J500-NaOH, and J500

Absorbent	Linear		Langmuir			Freundlich		
	K_d	R^2	q_m	b	R^2	K_F	$1/n$	R^2
J500-HNO_3	0.452	0.978	10.128	0.197	0.972	2.363	0.444	0.991
J500-NaOH	0.258	0.933	8.217	0.176	0.976	1.775	0.450	0.982
J500	0.137	0.977	6.919	0.206	0.968	0.711	0.562	0.994

modification, indicating that the maximum adsorption capacity had increased, and the adsorption performance had become stronger (Jin et al. 2018). The capacity factor K_F of the modified biochar had been accumulated and the adsorption of naphthalene was more stable. Both the acid and base treatment of biochar increased the functional groups which led to the enhancement of adsorption capacity. It was possible that HNO_3 leaching of biochar removed the ash and dredged the pore structure, thus optimizing its adsorption performance (Tang et al. 2017).

Conclusions

Among chicken manure–based biochar prepared by pyrolysis under three temperatures, J700 maintained a mesoporous pore structure as well as a relatively complete crystal structure. The four types of biochar demonstrated a high rate adsorption within 1 h after the process started, which was suitable for the simulation of pseudo-second-order kinetic equations. The adsorption capacity order was J500 ≈ JM500 < J300 < J700. Both adsorption equilibrium concentrations of four

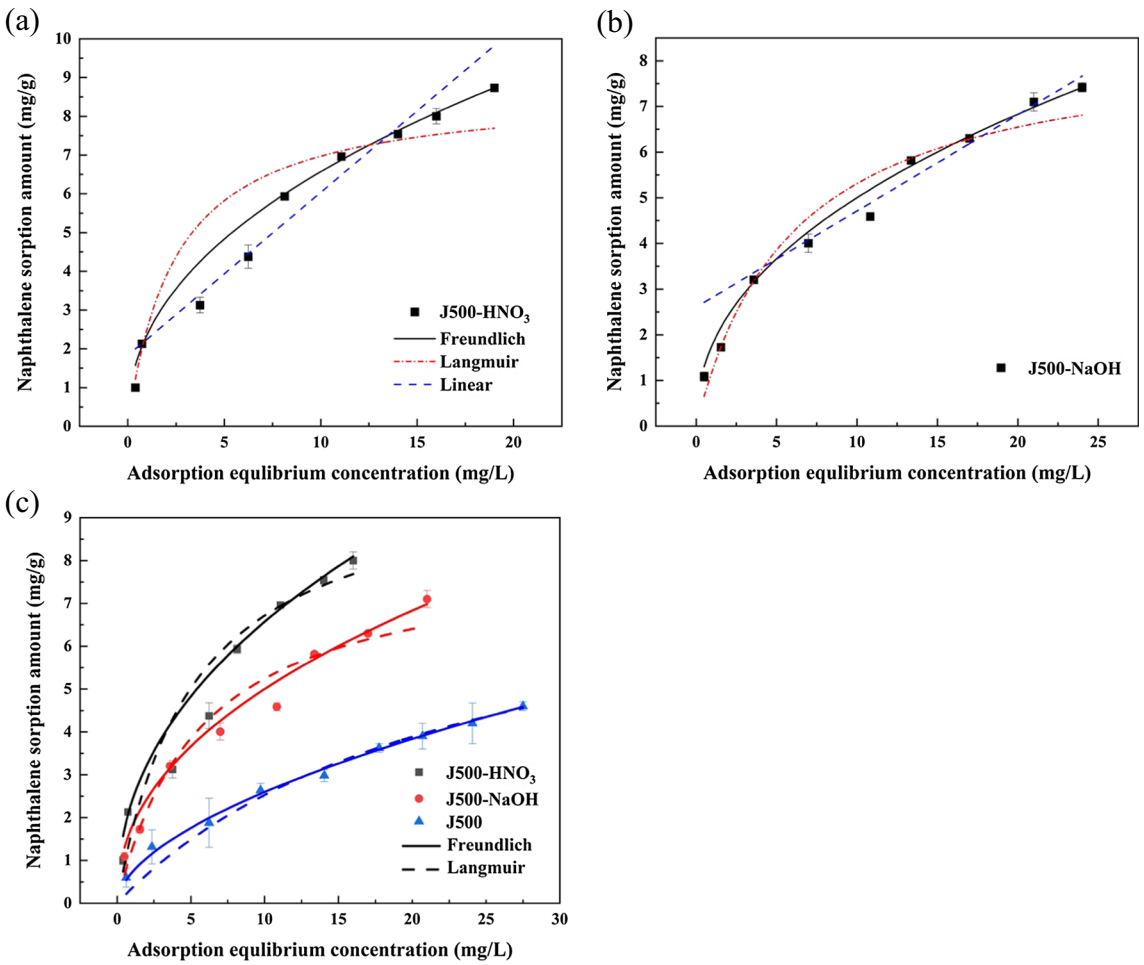

Fig. 6 Linear, Langmuir, and Freundlich isotherm models of naphthalene onto J500-HNO_3 (**a**) and J500-NaOH (**b**). **c** Langmuir and Freundlich isotherm models of naphthalene onto J500-HNO_3, J500-NaOH, and J500

kinds of biochar and the adsorption capacity of naphthalene increased, as the increase of the initial concentration of naphthalene. Naphthalene adsorption by biochar was more suitable for the fitting of the Freundlich model, indicating that chemical adsorption existed for the process. In addition to J700, the others were also suitable for Langmuir model fitting, indicating that there existed monolayer adsorption. J700 represented the best adsorption performance for the naphthalene removal from aqueous solutions. HNO_3-modified biochar kept more adsorption sites and enhanced chemisorption. NaOH-modified chemisorption had also been enhanced, but HNO_3 exposed a better modification effect.

Acknowledgments This work was financially supported by National Key R&D Program of China (2019YFC1803405; 2019YFD1101300).

Authors' contributions C.L. and Z.Y. designed and did the experiments, while D.H., F.M., and R.C. helped during the experiments. L.Z. and C.H. supervised the work.

Declarations This paper is our unpublished work and it has not been submitted to any other journal for reviews. Thus, it has not been previously published, in whole or in part, and it is not under consideration by any other journal.

Consent to publish All authors are aware of, and accept responsibility for, the manuscript.

Conflict of interest The authors declare that they have no conflict of interest.

References

Alade AO (2012) Adsorption of naphthalene onto activated carbons derived from milk bush kernel shell and flamboyant pod. J Environ Chem Ecotoxicol 4:124–132. https://doi.org/10.5897/jece11.041

Chen B, Chen Z (2009) Sorption of naphthalene and 1-naphthol by biochars of orange peels with different pyrolytic temperatures. Chemosphere 76:127–133. https://doi.org/10.1016/j.chemosphere.2009.02.004

Chen B, Zhou D (2008) Transitional adsorption and partition of nonpolar and polar aromatic contaminants by biochars of pine needles with different pyrolytic temperatures. Environ Sci Technol 42:5137–5143

Dai Y, Niu J, Yin L, Xu J, Xu J (2013) Laccase-carrying electrospun fibrous membrane for the removal of polycyclic aromatic hydrocarbons from contaminated water. Sep Purif Technol 104:1–8. https://doi.org/10.1016/j.seppur.2012.11.013

Fernandes A, Rose M, Falandysz J (2017) Polychlorinated naphthalenes (PCNs) in food and humans. Environ Int 104:1–13. https://doi.org/10.1016/j.envint.2017.02.015

Freddo A, Cai C, Reid BJ (2012) Environmental contextualisation of potential toxic elements and polycyclic aromatic hydrocarbons in biochar. Environ Pollut 171:18–24. https://doi.org/10.1016/j.envpol.2012.07.009

Gómez J, Alcántara MT, Pazos M, Sanromán MA (2010) Remediation of polluted soil by a two-stage treatment system: desorption of phenanthrene in soil and electrochemical treatment to recover the extraction agent. J Hazard Mater 173:794–798. https://doi.org/10.1016/j.jhazmat.2009.08.103

Hale SE, Lehmann J, Rutherford D et al (2012) Quantifying the total and bioavailable polycyclic aromatic hydrocarbons and dioxins in biochars. Environ Sci Technol 46(5):2830–2838

Harmsen J, Rietra RPJJ (2018) 25 years monitoring of PAHs and petroleum hydrocarbons biodegradation in soil. Chemosphere 207:229–238. https://doi.org/10.1016/j.chemosphere.2018.05.043

Jin J, Li S, Peng X, Liu W, Zhang C, Yang Y, Han L, du Z, Sun K, Wang X (2018) HNO 3 modified biochars for uranium (VI) removal from aqueous solution. Bioresour Technol 256:247–253. https://doi.org/10.1016/j.biortech.2018.02.022

Kaur V, Sharma P (2019) Effect of Prosopis juliflora biochar on physico-chemical properties of naphthalene and phenanthrene contaminated soil. Polycycl Aromat Compd 0:1–12. https://doi.org/10.1080/10406638.2019.1678185

Keiluweit M, Nico PS, Johnson MG (2010) Dynamic molecular structure of plant biomass-derived black carbon (biochar). Environ Sci Technol 44:1247–1253

Kumar A, Gupta H (2020) Activated carbon from sawdust for naphthalene removal from contaminated water. Environ Technol Innov 20:101080. https://doi.org/10.1016/j.eti.2020.101080

Lamichhane S, Bal Krishna KC, Sarukkalige R (2016) Polycyclic aromatic hydrocarbons (PAHs) removal by sorption: a review. Chemosphere 148:336–353. https://doi.org/10.1016/j.chemosphere.2016.01.036

Leng RA (2014) Interactions between microbial consortia in biofilms : a paradigm shift in rumen microbial ecology and enteric methane mitigation. Anim Prod Sci 54:519–543

Li C, Zhu X, He H, Fang Y, Dong H, Lü J, Li J, Li Y (2019) Adsorption of two antibiotics on biochar prepared in air-containing atmosphere: influence of biochar porosity and molecular size of antibiotics. J Mol Liq 274:353–361. https://doi.org/10.1016/j.molliq.2018.10.142

Lin Q, Xu X, Chen Q et al (2017) The speciation, leachability and bioaccessibility of Cu and Zn in animal manure-derived biochar: effect of feedstock and pyrolysis temperature. Front Environ Sci Eng 11:1–12. https://doi.org/10.1007/s11783-017-0924-8

Liu J, Chen J, Jiang L, Yin X (2014) Adsorption of mixed polycyclic aromatic hydrocarbons in surfactant solutions by activated carbon. J Ind Eng Chem 20:616–623. https://doi.org/10.1016/j.jiec.2013.05.024

Liu Y, Xu Y, Huang Q, Qin X, Zhao L, Liang X, Wang L, Sun Y (2019) Effects of chicken manure application on cadmium and arsenic accumulation in rice grains under different water conditions. Environ Sci Pollut Res 26:30847–30856. https://doi.org/10.1007/s11356-019-06271-y

Luo J, Li X, Ge C, Müller K, Yu H, Huang P, Li J, Tsang DCW, Bolan NS, Rinklebe J, Wang H (2018) Sorption of norfloxacin, sulfamerazine and oxytetracycline by KOH-modified biochar under single and ternary systems. Bioresour Technol 263:385–392. https://doi.org/10.1016/j.biortech.2018.05.022

Meng Y, Liu X, Lu S, Zhang T, Jin B, Wang Q, Tang Z, Liu Y, Guo X, Zhou J, Xi B (2019) A review on occurrence and risk of polycyclic aromatic hydrocarbons (PAHs) in lakes of China. Sci Total Environ 651:2497–2506. https://doi.org/10.1016/j.scitotenv.2018.10.162

Mirbagheri AANS, Chen ZHP (2019) Efficient removal of naphthalene from aqueous solutions using a nanoporous kaolin/Fe3O4 composite. Int J Environ Sci Technol 17:1991–2002. https://doi.org/10.1007/s13762-019-02521-1

Mirheidari A, Torbatinejad NM, Shakeri P, Mokhtarpour A (2019) Effects of walnut shell and chicken manure biochar on in vitro fermentation and in vivo nutrient digestibility and performance of dairy ewes. Trop Anim Health Prod 51:2153–2160. https://doi.org/10.1007/s11250-019-01909-y

Mohan D, Sarswat A, Ok YS, Pittman CU (2014) Organic and inorganic contaminants removal from water with biochar, a renewable, low

cost and sustainable adsorbent – a critical review. Bioresour Technol 160:191–202. https://doi.org/10.1016/j.biortech.2014.01.120

Mukherjee A, Zimmerman AR, Harris W (2011) Surface chemistry variations among a series of laboratory-produced biochars. Geoderma 163:247–255. https://doi.org/10.1016/j.geoderma.2011.04.021

Ncube S, Madikizela L, Cukrowska E, Chimuka L (2018) Recent advances in the adsorbents for isolation of polycyclic aromatic hydrocarbons (PAHs) from environmental sample solutions. Trends Anal Chem 99:101–116. https://doi.org/10.1016/j.trac.2017.12.007

Patra AK, Saxena J (2011) Exploitation of dietary tannins to improve rumen metabolism and ruminant nutrition. J Sci Food Agric 91: 24–37. https://doi.org/10.1002/jsfa.4152

Peluffo M, Rosso JA, Morelli IS, Mora VC (2018) Strategies for oxidation of PAHs in aged contaminated soil by batch reactors. Ecotoxicol Environ Saf 151:76–82. https://doi.org/10.1016/j.ecoenv.2017.12.067

Prak DJL, Pritchard PH (2002) Solubilization of polycyclic aromatic hydrocarbon mixtures in micellar nonionic surfactant solutions. Water Res 36:3463–3472. https://doi.org/10.1016/S0043-1354(02)00070-2

Shi W, Guo Y, Ning G, Li C, Li Y, Ren Y, Zhao O, Yang Z (2018) Remediation of soil polluted with HMW-PAHs by alfalfa or brome in combination with fungi and starch. J Hazard Mater 360:115–121. https://doi.org/10.1016/j.jhazmat.2018.07.076

Tang L, Yu J, Pang Y et al (2017) Sustainable efficient adsorbent: alkali-acid modified magnetic biochar derived from sewage sludge for aqueous organiccontaminant removal. Chem Eng J 336:160–169

Thang PQ, Jitae K, Giang BL, Viet NM, Huong PT (2019) Potential application of chicken manure biochar towards toxic phenol and 2, 4-dinitrophenol in wastewaters. J Environ Manag 251:109556. https://doi.org/10.1016/j.jenvman.2019.109556

Tian R, Li C, Xie S, You F, Cao Z, Xu Z, Yu G, Wang Y (2019) Preparation of biochar via pyrolysis at laboratory and pilot scales to remove antibiotics and immobilize heavy metals in livestock feces. J Soils Sediments 19:2891–2902. https://doi.org/10.1007/s11368-019-02350-2

Wang Z, Liu G, Zheng H, Li F, Ngo HH, Guo W, Liu C, Chen L, Xing B (2014) Investigating the mechanisms of biochar's removal of lead from solution. Bioresour Technol 177:308–317. https://doi.org/10.1016/j.biortech.2014.11.077

Wei J, Tu C, Yuan G, Liu Y, Bi D, Xiao L, Lu J, Theng BKG, Wang H, Zhang L, Zhang X (2019) Assessing the effect of pyrolysis temperature on the molecular properties and copper sorption capacity of a halophyte biochar. Environ Pollut 251:56–65. https://doi.org/10.1016/j.envpol.2019.04.128

Wu M, Pan B, Zhang D, Xiao D, Li H, Wang C, Ning P (2013) The sorption of organic contaminants on biochars derived from sediments with high organic carbon content. Chemosphere 90: 782–788. https://doi.org/10.1016/j.chemosphere.2012.09.075

Xu D, Cao J, Li Y, Howard A, Yu K (2019) Effect of pyrolysis temperature on characteristics of biochars derived from different feedstocks: a case study on ammonium adsorption capacity. Waste Manag 87:652–660. https://doi.org/10.1016/j.wasman.2019.02.049

Yao Y, Gao B, Chen H, Jiang L, Inyang M, Zimmerman AR, Cao X, Yang L, Xue Y, Li H (2012) Adsorption of sulfamethoxazole on biochar and its impact on reclaimed water irrigation. J Hazard Mater 209–210:408–413. https://doi.org/10.1016/j.jhazmat.2012.01.046

Yargicoglu EN, Yamini B, Reddy KR, Spokas K (2014) Physical and chemical characterization of waste wood derived biochars. Waste Manag 36:256–268. https://doi.org/10.1016/j.wasman.2014.10.029

Yin Z, Liu Y, Liu S, Jiang L, Tan X, Zeng G, Li M, Liu S, Tian S, Fang Y (2018) Activated magnetic biochar by one-step synthesis: enhanced adsorption and coadsorption for 17β-estradiol and copper. Sci Total Environ 639:1530–1542. https://doi.org/10.1016/j.scitotenv.2018.05.130

Yin Z, Liu Y, Tan X, Jiang L, Zeng G, Liu S, Tian S, Liu S, Liu N, Li M (2019) Adsorption of 17B-estradiol by a novel attapulgite/biochar nanocomposite: characteristics and influencing factors. Process Saf Environ Prot 121:155–164. https://doi.org/10.1016/j.psep.2018.10.022

Zeng AX, Xiao Z, Zhang G (2018) SC. Elsevier B.V.

Zhang ZL, Hong HS, Zhou JL, Yu G (2004) Phase association of polycyclic aromatic hydrocarbons in the Minjiang River Estuary, China. Sci Total Environ 323:71–86. https://doi.org/10.1016/j.scitotenv.2003.09.026

Zheng H, Wang Z, Deng X, Zhao J, Luo Y, Novak J, Herbert S, Xing B (2013a) Characteristics and nutrient values of biochars produced from giant reed at different temperatures. Bioresour Technol 130: 463–471. https://doi.org/10.1016/j.biortech.2012.12.044

Zheng H, Wang Z, Zhao J, Herbert S, Xing B (2013b) Sorption of antibiotic sulfamethoxazole varies with biochars produced at different temperatures. Environ Pollut 181:60–67. https://doi.org/10.1016/j.envpol.2013.05.056

Zhou W, Wang X, Chen C, Zhu L (2013) Removal of polycyclic aromatic hydrocarbons from surfactant solutions by selective sorption with organo-bentonite. Chem Eng J 233:251–257. https://doi.org/10.1016/j.cej.2013.08.040

Zhu L, Li S, Hu T, Nugroho YK, Yin Z, Hu D, Chu R, Mo F, Liu C, Hiltunen E (2019) Effects of nitrogen source heterogeneity on nutrient removal and biodiesel production of mono- and mix-cultured microalgae. Energy Conversion and Management 201:112144